An experimental and first-principle investigation of the Ca-substitution effect on P3-type layered NaxCoO2

Ishado, Yuji ; Hasegawa, Hirona ; Okada, Shigeto ; Mizuhata, Minoru ; Maki, Hideshi ; Matsui, Masaki

(Citation)
Chemical Communications,56(58):8107-8110

(Issue Date)
2020-07-25

(Resource Type)
journal article

(Version)
Accepted Manuscript

(URL)
https://hdl.handle.net/20.500.14094/90007369

COMMUNICATION

An experimental and first-principle investigation of the Ca-substitution effect on P3-type layered Na_xCoO_2†

Received 00th January 20xx,
Accepted 00th January 20xx

DOI: 10.1039/x0xx00000x

Yuji Ishado,[a] Hirona Hasegawa,[b] Shigeto Okada,[cd] Minoru Mizuhata,[be] Hideshi Maki,[b] and Masaki Matsui*[bd]

We experimentally and computationally investigated the Ca substitution effect on the electrochemical performance of P3-Na_xCoO_2. The cycle performance of Ca-substituted $Na_xCa_{0.05}CoO_2$ was effectively improved due to its better crystallinity retention after charging. Our DFT calculations suggested that the presence of Ca^{2+} ions in Na sites kinetically mitigates phase transition.

Over the last decade, Na-ion batteries (SIBs) have attracted much research interest as an alternative to Li-ion batteries due to the abundance and low cost of Na resources.[1] Layered sodium transition metal oxides, Na_xMO_2, are considered to be promising cathode active materials for SIBs, and they have been extensively studied.[2-8] However, the layered oxides exhibit phase transitions accompanied by MO_2 slab gliding during the charge/discharge process.[9, 10] Since the phase transition leads a capacity fading, various elemental substitutions of transition metals have been investigated to suppress the irreversible phase transitions during the charge/discharge process.[11-15] The phase transition can also be suppressed by replacing Na^+ ions (1.02 Å, CN = 6) with Ca^{2+} ions (1.0 Å, CN = 6) that have a similar ionic radius.[16, 17] We previously reported that the cycling performance of the P2-type $Na_{2/3}CoO_2$ is improved by Ca substitution.[18] Despite the improved cycling performance, the overpotential of the cathode increased because the doped Ca^{2+} ions hindered the Na^+ ion diffusion in the layered structure. The shrinkage of the lattice constant by the Ca substitution also interferes with the kinetics of Na^+ ions.

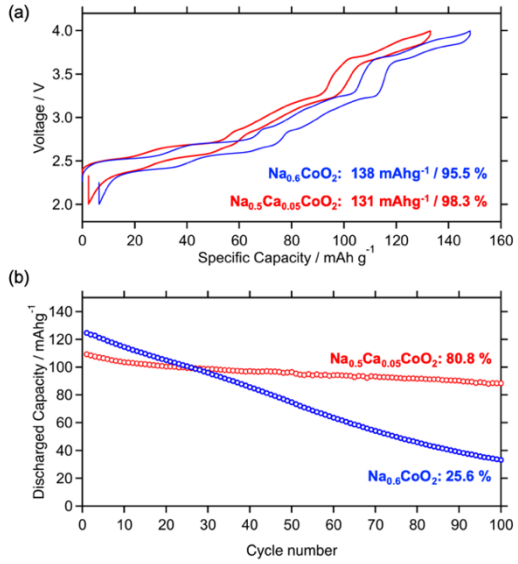

Fig. 1 Charge/discharge profiles of $Na_{0.81}CoO_2$ and $Na_{0.5}Ca_{0.05}CoO_2$ at the 3rd cycle (a). Cycle performance of $Na_{0.6}CoO_2$ and $Na_{0.5}Ca_{0.05}CoO_2$ (b).

Here we performed the synthesis of the Ca-substituted P3-type Na_xCoO_2 and confirmed that its cycling performance was improved without an increase in overpotential. *Ab-initio* calculations were also conducted to understand the Ca-substitution effect on the suppression of the phase transitions and the overpotential in the P3-type layered structure, which is classified as another structural group of the layered materials.[19]

The P3-type Na_xCoO_2 (NCO) and Ca-doped Na_xCoO_2 (NCCO) were synthesized by a conventional solid-state method (see the Supplementary Information for more detail). X-ray diffraction (XRD) patterns of the as-prepared NCO and NCCO are shown in Figure S1. All the diffraction peaks are indexed as P3-type NCO. The NCCO is also characterized as a P3 phase without any impurity phase. The Rietveld refinement result shows that the substituted Ca^{2+} ions preferably occupy the Na sites as shown in Figure S1 (b). The SEM-

[a] *Interdisciplinary Graduate School of Engineering Sciences, Kyushu University, Kasuga-koen 6-1, Kasuga 816-8580, Japan*
[b] *Department of Chemical Science and Engineering, Kobe University, Kobe, Japan*
[c] *Institute for Materials Chemistry and Engineering, Kyushu University, Kasuga-koen, Kasuga 816-8580, Japan*
[d] *Elements Strategy Initiative for Catalyst and Batteries (ESICB), Kyoto University, Japan*
[e] *Faculty of Chemistry, Jagiellonian University Gronostajowa 2, 30-387 Kraków, Poland*

† Electronic Supplementary Information (ESI) available. See DOI: 10.1039/x0xx00000x

‡ The 1st and 2nd authors are equally contributed to the paper.

EDX mapping shows the uniform distribution of Ca in the particles, which suggests that the Ca^{2+} ions are incorporated with Na^{+} ions in the van der Waals gap between layers (Figure S1 (c)). The actual Na content in the Ca-free and Ca-substituted materials are $Na_{0.81}CoO_2$ and $Na_{0.69}Ca_{0.04}CoO_2$, respectively.

The electrochemical properties of the NCO and NCCO were measured using a half-cell against Na metal counter electrodes. Figure 1 shows the charge/discharge profiles of NCO and NCCO at the 3rd cycle. Overall the charge/discharge profiles are in good agreement with the O3-type $NaCoO_2$ or P3-type Na_xCoO_2 reported in literature.[2, 15] The capacity of NCCO (131 mAh g^{-1}) is slightly smaller than that of NCO (138 mAh g^{-1}), but its lower capacity corresponds to the substituted Ca^{2+} ion content. Even though the substituted Ca^{2+} ions would be expected to hinder the migration of the Na^{+} ions, the NCCO shows even smaller hysteresis in the charge/discharge profile. The Ca substitution also improves the reversibility during the charge/discharge process. The Coulombic efficiency of the NCCO is 98.3%, while NCO shows a Coulombic efficiency of 95.5%. The improved Coulombic efficiency indicates that the irreversible phase transition at high voltage is suppressed by the Ca substitution. Moreover, the suppressed irreversibility brings to a significant improvement in cycling performances, as shown in Figure 1 (b). The NCCO shows capacity retention of 80.8% after 100 cycles, while the NCO shows severe capacity decay (capacity retention: 25.6%).

Next, to elucidate the origin of the capacity decay, we attempted to detect a trace of the irreversible phase transition by preparing overcharged cathodes. Figure 2 shows ex-situ XRD patterns of NCO and NCCO during the charging process. The structural evolution of the NCO is in good agreement with the past report. The NCO and NCCO show monoclinic O'3 phases at 2.6 V and transform to P3 and P'3 phases upon Na extraction. Another phase transition to the hexagonal O3' phase is observed around 3.9 V. We suppose the P'3 to O3' phase transition at high voltage leads to the significant capacity decay of the NCO. The capacity retention of the NCO operated at 2.0-3.7 V shows improved capacity retention of 66.7 %, as shown in Figure S3. Also, the poor crystallinity of the NCO charged up to 4.5 V indicates the irreversible phase transition shown in Figure S4. Hence, we suppose the Ca-substitution suppresses the irreversible phase transition of the NCO at the high voltage.

DFT calculations were also performed with the Vienna Ab Initio Simulation Package (VASP)[20, 21] to investigate the Ca-substitution effect on the phase stability of NCO (See the Supplementary Information for more details about the computational methods). We used supercells of $Na_xCo_{18}O_{36}$ and $Na_xCaCo_{18}O_{36}$ for the Ca-free and Ca-substituted materials, respectively. The Ca content of $Na_xCaCo_{18}O_{36}$, which is also represented as $Na_xCa_{0.056}CoO_2$, is slightly higher than that of the experimentally synthesized NCCO due to the limitation of the available Ca^{2+} ion sites in the supercells. Since the difference in the Ca content between the computational and experimental studies is small, we believe it does not affect the calculated properties such as phase stability.

Figure 3 (a,b) shows the calculated formation energies and the convex hulls of Na_xCoO_2 and $Na_xCa_{0.056}CoO_2$, respectively. Note that we use the Co oxidation state as an x-axis at the bottom so that it

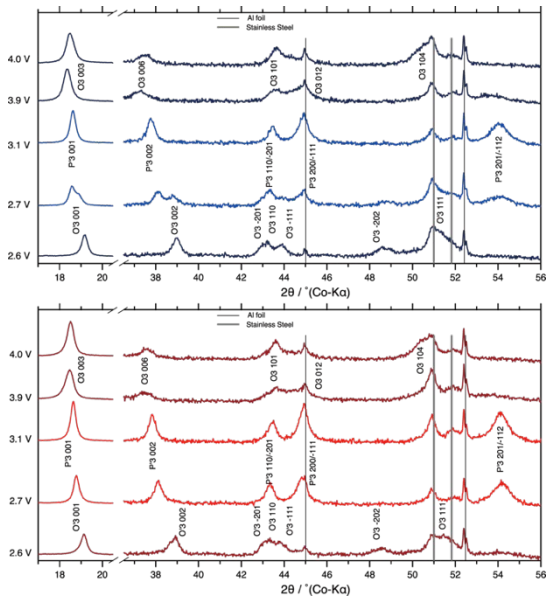

Fig. 2 ex-situ XRD patterns of Na_xCoO_2 (a) and $Na_xCa_{0.05}CoO_2$ (b) electrodes during the charging process.

enables the comparison of phase stability at the same oxidation state of Co. O1-CoO_2 and O3-$NaCoO_2$ are used as reference states for NCO, and O1-$Ca_{0.056}O_2$ and $Na_{0.889}Ca_{0.056}CoO_2$ are used as references for NCCO. The globally stable convex hulls are described with a solid black line. The areas shaded in red, green, and blue represent the ranges where the O1, O3, P3 structures are the most stable, respectively. The other areas are expected to be two-phase regions. The O3 phase is the most stable among the three structural types in the range of $1.0 \geq x \geq 0.833$ in the case of the Na_xCoO_2 (Fig. 3 (a)). Upon Na extraction from $NaCoO_2$, the P3 becomes the most stable phase at $0.667 \geq x \geq 0.444$. This result is consistent with both the past computational results[22] and the experimental results. The formation of the 2nd O3 phase (x = 0.333) is also in good agreement with the experimental results discussed above. Also, the O1 phase becomes thermodynamically favorable, at the fully desodiated composition (x=0), where the oxidation state of Co is 4.0. The region of $0.333 > x > 0$ is expected to be a two-phase region of the O3 and O1 phase. We suspect the origin of the peak broadening of the charged Na_xCoO_2 detected in Fig. 2 (a) is the O3- O1 phase transition.

The convex hull of the $Na_xCa_{0.056}CoO_2$ is shown in Fig. 3 (b). Since the mobility of the Ca^{2+} ions is presumably negligible compared with Na^{+} ions, the Ca^{2+} ions remain in the matrix even after the full extraction of Na^{+} ions. The estimated composition of the fully desodiated phase becomes $Ca_{0.056}CoO_2$. As a result, the highest oxidation state of Co in $Na_xCa_{0.056}CoO_2$ does not exceed 3.89. In addition, the oxidation state of the Co is not expected to be <3.0 in the voltage range in our electrochemical tests, and thus the maximum Na content is limited to 0.889, where the composition is $Na_{0.889}Ca_{0.056}CoO_2$.

In the convex hull of the $Na_xCa_{0.056}CoO_2$, the general trend of the phase stability is similar to that of the Na_xCoO_2. The structural evolution from O3, via P3 and O3 to O1, is consistent with Na_xCoO_2. Despite these general similarities, there are some minor variations.

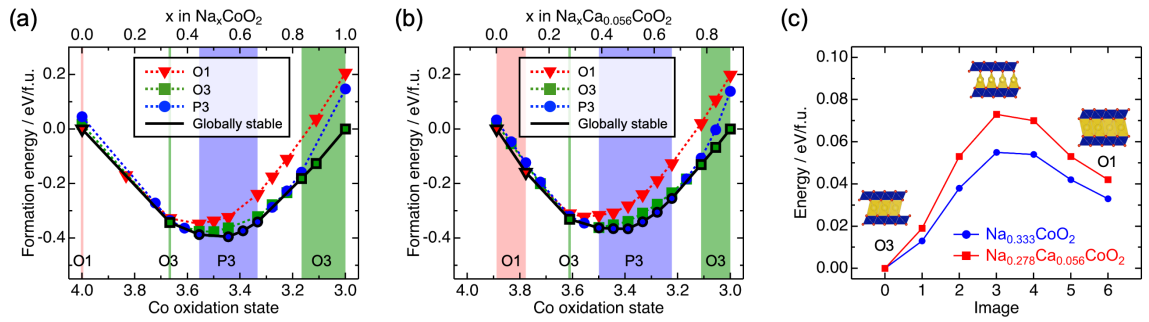

Fig. 3 Convex hulls of (a) Na_xCoO_2 and (b) $Na_xCa_{0.056}CoO_2$. (c) Estimated activation energies of the phase transition from O3 to O1. The compositions of the structures are $Na_{0.333-y}Ca_yCoO_2$ (y = 0 or 0.056). X-axis represents each image (structure) during the phase transition.

The stable region of the O3 phase at high Na content (x > 0.778) becomes narrow, while the P3- and O1-stable regions expand, compared with Na_xCoO_2. The expanded P3-stable region by the Ca-substitution is in consistent with the ex-situ XRD results shown in Figure 2.

In addition to studying the thermodynamic effect of the Ca substitution, we also investigated the kinetics of the phase transition by DFT calculation. Figure 3 (c) shows the estimated activation energies of the phase transition from O3 to O1 at the compositions of $Na_{0.333-y}Ca_yCoO_2$ (y = 0 or 0.056), which are the borders between the single O3 phase and O3-O1 two-phase region. Note that only two endpoints (O3 and O1) were fully relaxed, while the total energies of the intermediate states were calculated without any structural relaxation. Therefore, this calculation overestimates the actual activation energies; however, it enables us to elucidate the Ca-substitution effect qualitatively. The activation energy of the O3-O1 phase transition for $Na_{0.278}Ca_{0.056}CoO_2$ is higher than that for $Na_{0.333}CoO_2$. This result suggests that the divalent Ca^{2+} ions in the Na layer hinder the gliding of CoO_2 slabs. We attribute the improvement in the cycling performance of the Ca-substituted Na_xCoO_2 observed in our experiment above to the kinetically suppressed phase transition.

To investigate the Ca-substitution effect on Na ion diffusivity in the layered oxide, we calculated the migration energies of Na ions by the Climbing Image Nudged Elastic Band (CI-NEB) method.[23, 24] Figure 4 (a,b) illustrates migration paths of the Na ions in P3-$Na_{0.333}CoO_2$ and P3-$Na_{0.278}Ca_{0.056}CoO_2$, respectively. The numbers adjacent to the paths correspond to path1, path2, and path3, respectively. Note that the path1 and path2 are identical. The path3 is also identical to the path1 and path2, except the Ca site adjacent to the path instead of Na ion. Figure S5 also shows the migration paths from the different perspective. Fig 4 (c) displays the migration energy of each path. The migration energies of the path1, path2, and path3 are 319, 253, and 500 meV, respectively. The migration energy of path1 in P3-$Na_{0.333}CoO_2$ (319 meV) is higher than that for O3-$NaCoO_2$ (190 meV) and P3-$NaTiO_2$ (220 – 250 meV).[25, 26] This discrepancy is attributed to the different types of the structures (P3 and O3), the transition metals (Co and Ti) and the Na content (x ≈ 0.33 and x ≈ 1). The bottlenecks of these paths are located at around 60% of the path distance, where the hopping Na^+ ion passes by the adjacent alkali ion (Na^+ or Ca^{2+}).

The path2 has the lowest migration barrier among three paths. We attribute that the low migration barrier of the path2 is corresponding to the expansion of the Na layer along the c-axis. The calculated O-O bond lengths of the Na layer in $Na_{0.333}CoO_2$ and

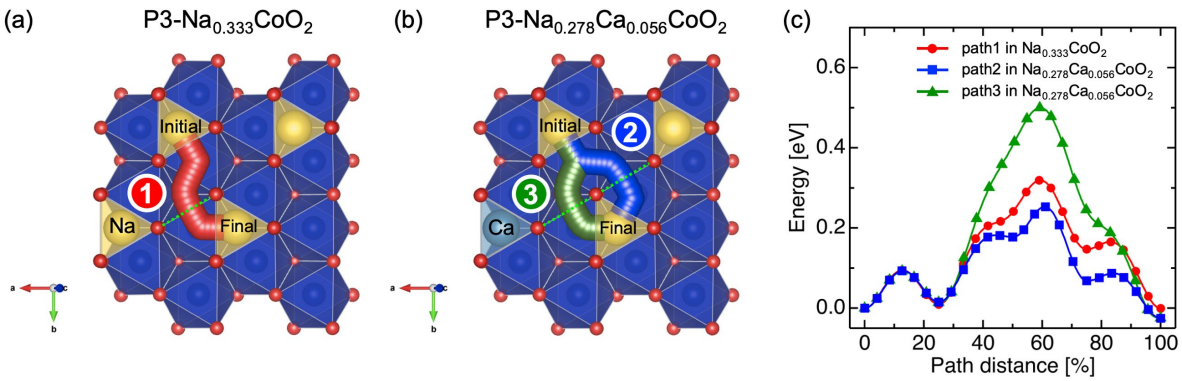

Fig. 4 Migration paths of Na ions in (a) P3-$Na_{0.333}CoO_2$ and (b) P3-$Na_{0.278}Ca_{0.056}CoO_2$. Yellow triangles and a light blue triangle represent the Na sites and a Ca site, respectively. The numbers adjacent to the paths represent path1, path2, and path3, respectively. The dotted green lines represent the bottlenecks of each path. (c) Migration barriers along each path.

$Na_{0.278}Ca_{0.056}CoO_2$ are 3.580 Å and 3.597 Å, respectively, as shown in Table S1. Figure S6 shows a coordination environment of a Na^+ ion in the P3 and P2-type structure. The NaO_6 prism in the P3 structure has a face-sharing CoO_6 octahedron on one side and three edge-sharing CoO_6 octahedra at another side. Once the Ca^{2+} ion occupies the Na site, the Na layer is expanded by the electrostatic repulsion between the divalent Ca^{2+} ion and the Co^{3+} ion at the face-sharing octahedron as shown in Fig. S6 (a). Therefore, the Ca substitution decreases the migration barrier of the Na^+ ions by expanding the bottleneck of the migration.

On the other hand, the migration barrier of the path3 (500 meV) is much larger than that of path1 (319 meV) and path2 (253 meV), because the Ca^{2+} ion electrostatically repels the Na^+ ion hopping at the neighboring prismatic site. Therefore, most of the Na^+ ions preferably take the path2 to avoid the adjacent prismatic site occupied by the Ca^{2+} ion.

A comparison with the Ca substitution in the P2-type layered structure is also helpful to understand the decreased migration energy of the path2 in the P3 phase. The P2-type structure has two identical sites: 2*b* and 2*d* sites, for the Na^+ ion. The 2*b* site has two face-sharing CoO_6 octahedra, while the 2*d* site has six edge-sharing CoO_6 octahedra. Since the Ca^{2+} ion preferably occupies the 2*d* site (Fig. S5 (b)), the lattice constant along the c-axis shrinks by the Ca substitution. Therefore, the Ca substitution in the P2 phase significantly increases the overpotential, as we previously reported.[18] Moreover, the overpotential of the P3-type $Na_xCa_{0.04}CoO_2$ does not become higher than that of P3-Na_xCoO_2. This result suggests the Ca substitution in the P3 phase partially promotes the Na^+ diffusion rather than limiting the Na^+ diffusion paths.

In summary, the Ca-substitution effect on P3-type Na_xCoO_2 was investigated. We found that the Ca substitution suppresses the irreversible phase transition at high voltage during the charging/discharging process, resulting in a significant improvement in the cycling performance compared with the Ca-free P3-Na_xCoO_2. Our DFT calculations suggest that the Ca substitution in P3-Na_xCoO_2 expands the stable region of the Na-diffusive P3 phase. Also, the presence of Ca^{2+} ions in the Na layer kinetically hinders the phase transition from O3 to O1, which is accompanied by the gliding of CoO_2 slabs. The suppressed phase transition leads to better crystallinity during the charge/discharge cycles. Our DFT-NEB calculations further proved that the Ca substitution decreases the migration barrier of the Na^+ ions, because the Ca^{2+} ions expand the bottleneck of the Na layers. We believe that Ca substitution could be a practical materials design strategy for improving the structural stability and rate capability of Na-based cathode active materials.

Acknowledgement

This work was partially supported by Element Strategy Initiative of MEXT, Grant Number JPMXP0112101003, and KAKENHI of MEXT, Grant Number 19H05813. The computation was carried out using the computer resource offered under the category of General Projects by Research Institute for Information Technology, Kyushu University.

Conflicts of interest

There are no conflicts to declare.

Notes and references

1. N. Yabuuchi, K. Kubota, M. Dahbi and S. Komaba, *Chem Rev*, 2014, **114**, 11636-11682.
2. C. Delmas, J.-J. Braconnier, C. Fouassier and P. Hagenmuller, *Solid State Ionics*, 1981, **3–4**, 165-169.
3. M. H. Han, E. Gonzalo, G. Singh and T. Rojo, *Energy & Environmental Science*, 2015, **8**, 81-102.
4. J.-J. Braconnier, C. Delmas, C. Fouassier and P. Hagenmuller, *Materials Research Bulletin*, 1980, **15**, 1797-1804.
5. A. Maazaz, C. Delmas and P. Hagenmuller, *Journal of Inclusion Phenomena*, 1983, **1**, 45-51.
6. X. Xia and J. R. Dahn, *Electrochemical and Solid-State Letters*, 2012, **15**, A1.
7. X. Xia and J. R. Dahn, *Journal of The Electrochemical Society*, 2012, **159**, A647.
8. N. Yabuuchi, H. Yoshida and S. Komaba, *Electrochemistry*, 2012, **80**, 716-719.
9. M. D. Radin, J. Alvarado, Y. S. Meng and A. Van der Ven, *Nano Letters*, 2017, **17**, 7789-7795.
10. X. Ma, H. Chen and G. Ceder, *Journal of The Electrochemical Society*, 2011, **158**, A1307.
11. I. Saadoune, A. Maazaz, M. Ménétrier and C. Delmas, *Journal of Solid State Chemistry*, 1996, **122**, 111-117.
12. Z. Lu, R. A. Donaberger and J. R. Dahn, *Chemistry of Materials*, 2000, **12**, 3583-3590.
13. S. Komaba, N. Yabuuchi, T. Nakayama, A. Ogata, T. Ishikawa and I. Nakai, *Inorganic chemistry*, 2012, **51**, 6211-6220.
14. X. Li, D. Wu, Y.-N. Zhou, L. Liu, X.-Q. Yang and G. Ceder, *Electrochemistry Communications*, 2014, **49**, 51-54.
15. K. Kubota, T. Asari, H. Yoshida, N. Yaabuuchi, H. Shiiba, M. Nakayama and S. Komaba, *Advanced Functional Materials*, 2016, **26**, 6047-6059.
16. S. C. Han, H. Lim, J. Jeong, D. Ahn, W. B. Park, K.-S. Sohn and M. Pyo, *Journal of Power Sources*, 2015, **277**, 9-16.
17. L. Sun, Y. Xie, X.-Z. Liao, H. Wang, G. Tan, Z. Chen, Y. Ren, J. Gim, W. Tang, Y.-S. He, K. Amine and Z.-F. Ma, *Small*, 2018, **14**, 1704523.
18. M. Matsui, F. Mizukoshi and N. Imanishi, *Journal of Power Sources*, 2015, **280**, 205-209.
19. C. Delmas, C. Fouassier and P. Hagenmuller, *Physica B*, 1980, **99**, 81-85.
20. G. Kresse and J. Furthmüller, *Computational Materials Science*, 1996, **6**, 15-50.
21. G. Kresse and J. Furthmüller, *Physical Review B*, 1996, **54**, 11169-11186.
22. J. L. Kaufman and A. Van der Ven, *Phys Rev Mater*, 2019, **3**, 015402.
23. G. Henkelman and H. Jónsson, *The Journal of Chemical Physics*, 2000, **113**, 9978-9985.
24. G. Henkelman, B. P. Uberuaga and H. Jónsson, *The Journal of Chemical Physics*, 2000, **113**, 9901-9904.
25. S. P. Ong, V. L. Chevrier, G. Hautier, A. Jain, C. Moore, S. Kim, X. Ma and G. Ceder, *Energy & Environmental Science*, 2011, **4**, 3680–3688.
26. S. Guo, Y. Sun, J. Yi, K. Zhu, P. Liu, Y. Zhu, G. Zhu, M. Chen, M. Ishida and H. Zhou, *NPG Asia Materials*, 2016, **8**, e266.

